# Ni-induced local distortions in $La_{1.85}Sr_{0.15}Cu_{1-y}Ni_yO_4$ and their relevance to $T_c$ suppression: An angular-resolved XAFS study

Daniel Haskel
*Experimental Facilities Division, Advanced Photon Source, Argonne National Laboratory, Argonne, Illinois 60439*

Edward A. Stern
*Department of Physics, Box 351560, University of Washington, Seattle, Washington 98195*

Victor Polinger
*School of Physics and Astronomy, University of Nottingham, Nottingham NG7 2RD, United Kingdom*

Fatih Dogan
*Department of Materials Science and Engineering, Box 352120, University of Washington, Seattle, Washington 98195*

(Received 12 October 2000; revised manuscript received 20 April 2001; published 21 August 2001)

We present results from angular-resolved x-ray-absorption fine-structure (XAFS) measurements at the Ni, La, and Sr $K$ edges of oriented powders of $La_{1.85}Sr_{0.15}Cu_{1-y}Ni_yO_4$, with $y=0.01$, 0.03, 0.06. A special magnetic alignment procedure allowed us to measure pure $\hat{c}$- and $ab$-oriented XAFS at the Ni $K$ edge in identical fluorescence geometries. Both the x-ray-absorption near-edge structure and the XAFS unequivocally show that the $NiO_6$ octahedra are contracted along the $c$ axis by $\approx 0.32$ Å relative to $CuO_6$ octahedra while the in-plane distances of $NiO_6$ and $CuO_6$ octahedra are the same within 0.01 Å. The $NiO_6$ octahedral contraction drives the average $\hat{c}$ axis contraction measured by diffraction with increasing content of Ni. The local $\hat{c}$ axis shows strong spatial fluctuations, due to the different $NiO_6$ and $CuO_6$ octahedral configurations and the stronger bonding of a $La^{3+}$ ion than a $Sr^{2+}$ ion to the O(2) apical oxygens of such octahedra. We discuss the relevance of these findings to the mechanisms of loss of superconductivity at $y\approx 0.03$ and hole localization above $y\approx 0.05$ by Ni dopants.

DOI: 10.1103/PhysRevB.64.104510 PACS number(s): 74.72.Dn, 74.80.−g, 61.10.Ht

## I. INTRODUCTION

The suppression of superconductivity in optimally doped $La_{1.85}Sr_{0.15}CuO_4$ by addition of the Cu substituting Ni and Zn atoms is quite dramatic. A replacement of only 3% of Cu atoms by Ni destroys superconductivity while 5% of Ni causes a metal-insulator transition.[1] Understanding the origin of this effect has been the focus of many recent investigations.[2–9] Since the lattice perturbation induced by the dopants was previously unknown the effect of structural distortions around impurities was only accounted for phenomenologically, e.g., by means of an increased effective mass of the quasiparticles that renormalizes the strength of the impurity potential.[4] This phenomenological approach was used in systematic studies of the effect of the impurity potential upon the superconducting state, in particular to predict the momentum dependence of the superconducting gap ($d$ wave versus isotropic $s$ wave) by studying the tunneling conductance in the neighborhood of impurities.[4,5] These studies, although highly instructive, neglect the details of the perturbation on the atomic scale. These details are also neglected in microscopic treatments, such as in Hubbard models[6,7] or in the $t$-$V$ model used by Martin and Balatsky.[8] In the latter the strength of the impurity potential is fitted to reproduce the energy position of impurity levels in the superconducting gap. Since the superconducting coherence length of high-$T_c$ cuprates is very short (a few interatomic distances) the details of the perturbation can be quite important.

To try to learn about superconductivity by destroying it with dopants might seem, at first, a rather negative approach. However, the work of Pan *et al.* demonstrated just the opposite,[10] and our angular-resolved x-ray-absorption fine-structure (XAFS) measurements supplement and reinforce their conclusions. In their scanning tunneling microscopy (STM) experiments on $T_c$-suppressed Zn-doped $Bi_2Sr_2CaCu_2O_8$ at temperatures below $T_c$, no quasiparticle tunneling current was obtained at zero bias for most of the STM tip locations on the cleaved BiO surface, as expected due to the presence of a superconducting gap. However, a zero-bias tunneling current was measured when the STM tip was located precisely above a Zn dopant (two layers below the BiO surface) indicating the presence of an impurity state at the Zn dopant sites. At the same time the superconducting (SC) coherence peaks and gap magnitude are suppressed at these same sites. By mapping the spatial extent of the Zn impurity state away from its lattice site in different directions (by measuring the tunneling strength as a function of tip displacement away from the dopant), a $d$-wave-like dependence was obtained, the impurity state extending most strongly along the *nodes* of the SC gap. This spatial dependence agrees with theoretical predictions.[4,11] An additional, weaker, tunneling signal corresponding to an impurity state extending *along* the SC gap was also detected. Balatsky proposed that this weaker signal is due to enhanced tunneling between layers along the Cu-O bond directions.[11] More recently this spatial dependence was explained in terms of the

 

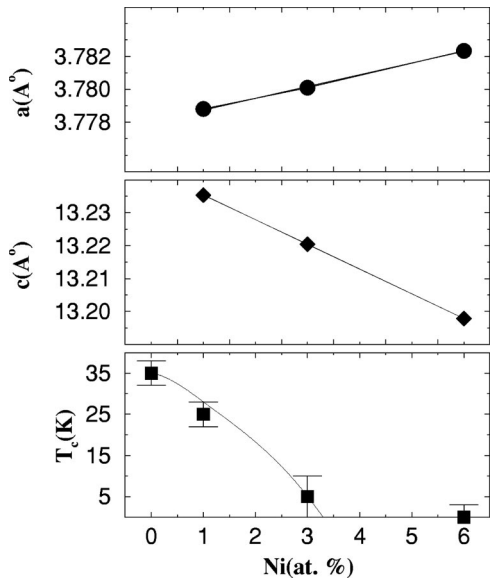


FIG. 1. Room-temperature lattice parameters and $T_c$'s for $La_{1.85}Sr_{0.15}Cu_{1-y}Ni_yO_4$. The value of $T_c$ at $y=0$ is from Radaelli *et al.* (Ref. 16).

different spatial distributions around the impurity of hole and electron contents of the quasiparticle excitations; i.e., in terms of the spinor wave functions of bound Bogoliubov quasiparticles.[8,9]

Clearly the local structure around dopants will influence the nature of the impurity states. Electronic states at the Fermi level are derived from O $2p$ and Cu $3d$ atomic orbitals whose hybridization is a strong function of the relative Cu-O distances. Local distortions around dopants (and related changes in local electronic structure) will affect the tunneling matrix elements at a dopant site, compared to those at a neighboring Cu site. Orbital overlap and related hopping of carriers between sites, both in the $CuO_2$ plane and in its perpendicular direction, strongly depend on the details of the local distortions. It is therefore of importance to obtain detailed information on the local environment of the dopants when interpreting information from other spectroscopies at the atomic level. The XAFS technique is unique in that it can directly determine the local distortions around dilute dopants. Here we report on the nature of such distortions around Ni atoms. We show that local distortions around Ni atoms are predominately in the *out*-of-plane direction with negligible (within XAFS accuracy) in-plane effects on the local environment.

## II. EXPERIMENT

Powders of $La_{1.85}Sr_{0.15}Cu_{1-y}Ni_yO_4$ with $y=0.01$, 0.03, 0.06 were obtained by combustion synthesis from nitrate solutions.[12] Sintering of powder compacts ($\approx$3 g) took place at 1140 °C for 24 h. Lattice parameters were refined at room temperature using 14 Bragg reflections of the $I4/mmm$ space group. Superconducting $T_c$'s were obtained from zero-field-cooled magnetization curves measured by superconducting quantum interference device magnetometry in a $H=1$ Gauss applied field. Figure 1 shows the results from these measurements.

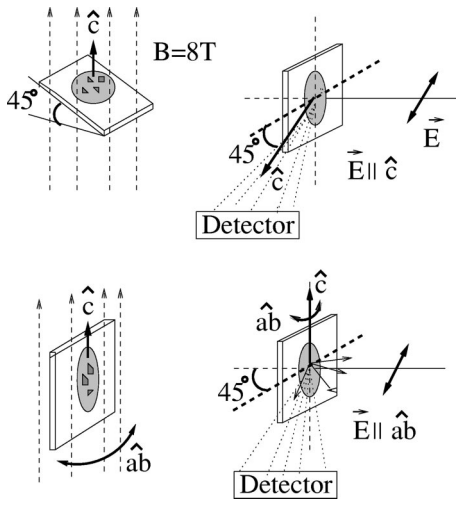


FIG. 2. Magnetic alignment geometry. Having the crystallographic $\hat{c}$ axis forming a 45° angle with the sample surface allowed measuring pure *c*-axis Ni *K*-edge fluorescence ($\hat{E}\|\hat{c}$) with the sample surface forming a 45° angle with the x rays' electric field (top panel). For the $\hat{E}\|$ $ab$-plane fluorescence measurements at the Ni *K* edge (and transmission measurements in both orientations at the Sr and La *K* edges) samples were aligned with the $\hat{c}$ axis in the plane of the sample (bottom panel).

XAFS measurements were taken on magnetically aligned powders. A general description of the alignment procedure is given in Ref. 12. This procedure results in powders aligned along their $\hat{c}$ axis but randomly oriented in the $ab$ plane.

The main advantage of this method over the use of single crystals is control over sample thickness, allowing the use of transmission geometry at the absorption edges of concentrated elements instead of the noisier fluorescence technique required for the x-ray opaque single crystals. It also allows controlling the orientation of the $\hat{c}$ axis relative to the sample's surface. The latter allowed us to measure pure $\hat{c}$-axis and $ab$-plane orientations at the Ni *K* edge in identical fluorescence geometries (Fig. 2) which give less noisy data for *dilute* dopants. Measurements were done in fluorescence at the Ni *K* edge and transmission at the Sr, La *K* edges at beamline X11-A of the National Synchrotron Light Source using Si(111) (Ni, Sr *K* edges) and Si(311) (La *K* edge) double-crystal monochromators. Ni *K*-edge XAFS is limited to about $\approx 13$ $Å^{-1}$ due to the appearance of Cu *K* edge in the absorption spectra.

Raw absorption data at the Ni *K* edge of $La_{1.85}Sr_{0.15}Cu_{1-y}Ni_yO_4$ with $y=0.06$ at $T=10$ K are shown in Fig. 3 for both orientations of the electric field; the near-edge region of the same data, obtained after preedge subtraction and edge-step normalization is emphasized in the main panel of the same figure.

## III. ANALYSIS AND RESULTS

Data analysis was carried out with the UWXAFS analysis package[13] together with theoretical standards from FEFF6.[14]

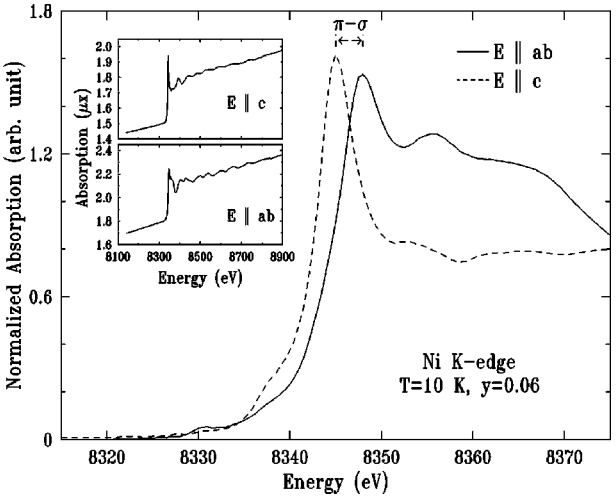


FIG. 3. Ni $K$-edge absorption spectra for $y=0.06$ at $T=10$ K measured in fluorescence geometry with $\hat{E}\|\hat{c}$ (top inset) and $\hat{E}\|ab$-plane (bottom inset) orientations. Main panel shows x-ray-absorption near-edge spectra obtained from the same data after preedge removal and edge-step normalization. The $4p_{\pi}$-$4p_{\sigma}$ energy splitting is determined by the distortion of the $NiO_6$ octahedron.

The orientation dependence of the XAFS signal was included in the FEFF6 calculations by performing the appropiate angular averaging for powder aligned along the $\hat{c}$ axis but randomly oriented in the $ab$ plane.[12] Data from both electric-field orientations ($\hat{E}\|\hat{c}$, $\hat{E}\|$ $ab$ plane) were analyzed concomitantly by constraining the structural parameters of scattering paths that contribute in both orientations to be the same, significantly reducing the number of fitting parameters relative to the number of independent points in the data. Coordination numbers were set to the values of the average structure determined by crystallography for Ni-undoped $La_{1.85}Sr_{0.15}CuO_4$.[16]

Fits were performed in real space by refining the structural parameters in the FEFF6 theoretical standard against the experimental data by a nonlinear least-squares minimization of a reduced $\chi^2_\nu$ statistic.[13] Multiple scattering (MS) paths that contribute to the XAFS in the fitted region were included in the fits. Uncertainties in the parameters are calculated by the change needed to increase $\chi^2_\nu$ by $1/\nu$ from its minimum value (one standard deviation) and include the effect of correlations between fitting parameters. Here $\nu$ are the degrees of freedom in the fit. Statistical errors are renormalized to account for systematic errors in the theory and the data. We found that systematic errors dominate our uncertainties, being approximately four times larger than random errors. More details on analysis procedures and error estimates are given in Refs. 12 and 15.

Figure 4 shows fit results at the Ni $K$ edge for both electric-field orientations. Structural parameters derived from the fits in Fig. 4 are summarized in Table I. Although we show here fitting results for a Ni-doping level of $y=0.06$, no significant differences were found in the fitted values for the lower Ni dopings. The Ni-O(2) apical distance is 0.16(1)-Å shorter than the corresponding Cu-O(2) apical distance. The Ni-O(1) planar distance is nearly unchanged relative to the

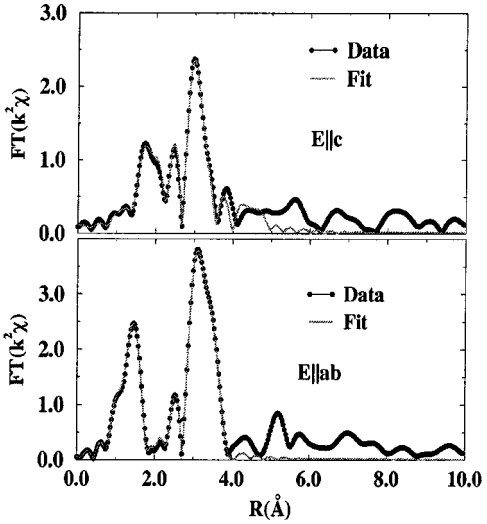


FIG. 4. Magnitude of the complex Fourier transform of $k^2\chi(k)$ for the Ni $K$ edge in $La_{1.85}Sr_{0.15}Cu_{1-y}Ni_yO_4$ with $y=0.06$ at $T=10$ K. The $k$ range used in the transform is [2.5–12.0] $Å^{-1}$; fitting ranges are [1.45–5.0] Å and [1.2–4.2]Å for $\hat{E}\|\hat{c}$ and $\hat{E}\|ab$ planes, respectively. Number of fitting parameters in the constrained fit of both orientations is 16, compared to a total of 45 independent points in the fitted region. The amplitude reduction factor is $S_0^2=0.902\pm0.067$; figures of merit for these fits are a statistical $\chi^2_\nu=15.8$ and a misfit fraction $R=0.006$. For a definition of these figures of merit see Ref. 13. Systematic errors are included by multiplying the random errors by $\chi_\nu\sim4$.

Cu-O(1) distance, although a relative expansion of the former by $\lesssim0.01$ Å cannot be ruled out based on the slightly larger Ni-Cu planar distance and the measured uncertainties. Ni-O(1)-Cu MS paths contribute to the XAFS at nearly the same distance as Ni-Cu single-scattering (SS) paths and are included in the fits. As the O(2) apical moves towards Ni, it drags along its neighbor La atom, as seen by the $\approx0.06$-Å contraction in Ni-$La_c$ distance. Here the $c$ subscript indicates that the Ni-La distance is nearly oriented along the $\hat{c}$ axis. Ni-O(2)-$La_c$ MS paths contribute at nearly the same distance as Ni-$La_c$ SS paths and are included in the fits.

The buckling angle $\alpha$ of the Ni-O(1)-Cu planar, nearly collinear, configuration was determined by fitting a parametrized form of the effective scattering amplitudes of double- and triple-scattering paths, $F_k(\alpha)$, to the data. The parametrization was done by simulating the buckling-angle depen-

TABLE I. Selected fitting results at the Ni $K$ edge. Data correspond to $y=0.06$ at $T=10$ K; the amplitude reduction factor is $S_0^2=0.902\pm0.067$. Diffraction results for the undoped ($y=0$) structure are from Radaelli *et al.* (Ref. 16). The Ni/Cu-$La_c$ distance is nearly oriented along the $\hat{c}$ axis.

| | XAFS | | Diffraction |
|---|---|---|---|
| Ni-O(1) | 1.882(08) Å | Cu-O(1) | 1.888 Å |
| Ni-Cu(planar) | 3.789(06) Å | Cu-Cu(planar) | 3.774 Å |
| Ni-O(2) | 2.250(12) Å | Cu-O(2) | 2.415 Å |
| Ni-$La_c$ | 4.701(16) Å | Cu-$La_c$ | 4.760 Å |

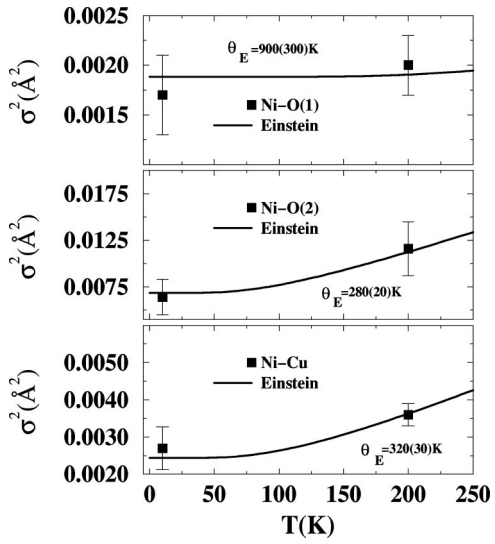


FIG. 5. Temperature dependence of the mean-squared disorder in selected interatomic distances around Ni atoms together with their fits to Einstein models. The mean-squared disorder in these bonds is solely of thermal origin without any evidence for a static contribution.

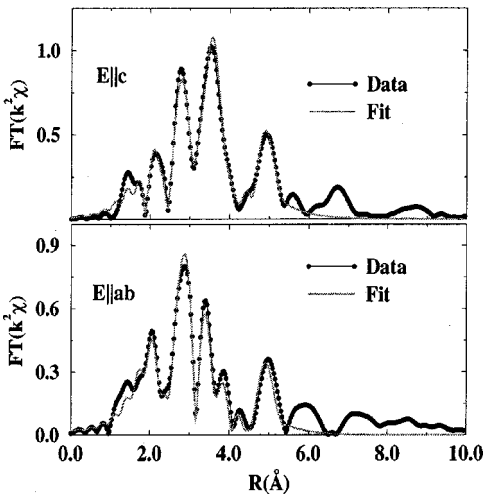


FIG. 6. Magnitude of complex Fourier transform of $k^2\chi(k)$ for La $K$ edge at $T=10$ K and $y=0.06$. Data range used in the transform is [3–14] $Å^{-1}$; fitting range is [1.5–5.2] Å for both orientations. The constrained fit of both orientations uses 22 fitting parameters compared to 52 independent points in the fitted region. Amplitude reduction factor is $S_0^2=0.93(6)$; figures of merit are a statistical $\chi_\nu^2=14.89$ and a misfit fraction $R=0.008$.

dence of such amplitudes in FEFF6 calculations (for a detailed description of this procedure see Ref. 12). The fitted value of $\alpha=2.5\pm3°$ is in agreement with the average buckling angle determined by diffraction, $\langle\alpha\rangle=3.61°$, indicating again that the local structural disorder introduced by Ni in the $CuO_2$ planes is small. The large uncertainty obtained in the fits of the buckling angle $\alpha$ is due to the small variation of $F_k(\alpha)$ for small buckling angles near collinearity ($0\leqslant\alpha\leqslant5°$).

Whether there is a spatial correlation between the positions of the two types of dopants (Ni, Sr) can be determined from Ni $K$-edge XAFS by fitting the Ni-(La/Sr) XAFS signal with varying amounts of Sr/La neighbors to Ni. Sr and La have very different backscattering amplitudes allowing separation of their isolated contributions to the XAFS. A fit to the Ni-(La/Sr) signal determines a relative Sr concentration of $x=0.048\pm0.06$. The relatively large uncertainty is due to the small fraction of Sr atoms coupled to the weaker backscattering amplitude of Sr compared to that of La atoms. For a random solution one expects $x=0.075$, while if Sr avoids Ni one expects $x=0$. The fitted value is consistent with either one of these scenarios, due to the relatively large uncertainty. However, *we can definitely rule out a strong tendency of Sr to occupy sites near Ni atoms.*[17]

Fitted values for the mean-squared disorder in selected interatomic distances at $T=10$, 200 K together with their parametrization to an Einstein model are shown in Fig. 5. We found no evidence for a static contribution to the mean-squared disorder in these distances. The much weaker effective force constant of the Ni-O(2) apical bond compared to that of the Ni-O(1) planar bond is evident from the much larger temperature dependence of the former. This weaker bonding allows the O(2) apical to relax towards the $Ni^{2+}$ ion while the strongly covalent Ni-O(1) bonding opposes the relaxation of O(1) atoms, thus preventing a true anti-Jahn-Teller distortion at the Ni site to materialize, as discussed below.

The x-ray-absorption near-edge structure (XANES) spectra shown in Fig. 3 fully support the XAFS results regarding the distortion of the $NiO_6$ octahedra. The ratio of the out-of-plane Ni-O(2) apical distance, $r_\parallel$, to the in-plane Ni-O(1) distance, $r_\perp$, $S=r_\parallel/r_\perp$, determines the $4p_\pi$-$4p_\sigma$ energy splitting shown in Fig. 3. This is because the hybridization-driven energy splitting of bonding and antibonding states for Ni-O(2) bonds along the $\hat{c}$-axis and Ni-O(1) bonds within the plane scales as $1/r_\parallel^2$ and $1/r_\perp^2$, respectively, as empirically determined in extensive studies of La cuprates and La nickelates by Oyanagi *et al.*,[18] Kosugi *et al.*,[19] and Sahiner *et al.*[20] X-ray absorption probes only the antibonding states, which are partially empty. Sahiner *et al.* summarized the measured $4p_\pi$-$4p_\sigma$ energy splitting for a series of cuprates and nickelates with known octahedral distortions. This splitting varies linearly with the distortion parameter $1/S^2$.[20] By interpolating our measured splitting of 3.0 eV into their curve, we obtain a distortion parameter $1/S^2=0.71$ or $S=r_\parallel/r_\perp=1.19$. This is in excellent agreement with the XAFS result of $S=1.19(1)$.

Fits to La $K$-edge XAFS data are shown in Fig. 6. The averaged local $\hat{c}$ axis, as obtained by averaging over all La sites, is given by the sum $2\times[\text{La-(Cu/Ni)}_c]+[\text{La-(La/Sr)}_c]$, where La-$(\text{Cu/Ni})_c$ and La-$(\text{La/Sr})_c$ bonds nearly coincide with the $\hat{c}$ axis. Ni-induced changes in this averaged local $\hat{c}$ axis should be in good agreement with the results of diffraction. Small deviations might occur since the actual local $\hat{c}$ axis has contributions from both La-$(\text{Cu/Ni})_c$ and La-$(\text{La/Sr})_c$ distances, as well as from Sr-$(\text{Cu/Ni})_c$ and Sr-$(\text{La/Sr})_c$ distances, their relative weights determined by the relative concentrations of La (92.5%) and Sr (7.5%). As

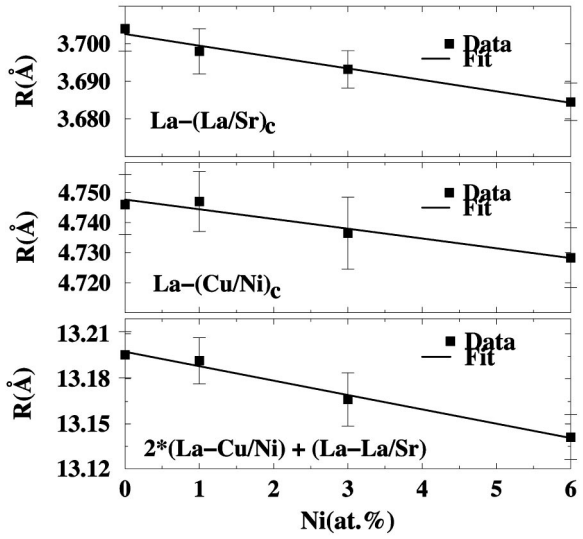


FIG. 7. The local $\hat{c}$ axis, averaged over all La sites, as determined from La *K*-edge XAFS at $T=10$ K as a function of Ni doping. The rate of contraction is in good agreement with the $\hat{c}$-axis contraction determined from powder-diffraction measurements at 300 K. $y=0$ results are from Ref. 22.

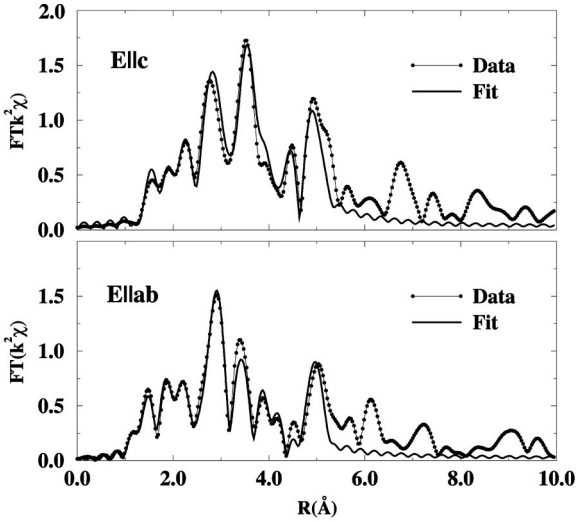


FIG. 8. Magnitude of complex Fourier transform of $k^2\chi(k)$ for Sr *K* edge at $T=10$ K and $y=0.06$. Data range used in the transform is $[3-14]$ Å$^{-1}$; fitting range is [1.5–5.2] Å for both orientations. The constrained fit of both orientations uses 22 fitting parameters compared to 52 independent points in the fitted region. Amplitude reduction factor is $S_0^2=1.08(10)$; figures of merit are a statistical $\chi_\nu^2=15.6$ and a misfit fraction $R=0.022$.

discussed below, these Sr distances show a slower rate of contraction with Ni than the La distances, and therefore the local $\hat{c}$-axis contraction rate determined from only the La sites is slightly overestimated. Figure 7 shows the rate of contraction, with Ni doping, of the local $\hat{c}$ axis as determined from La *K*-edge XAFS, at $T=10$ K. This rate is found to be $(dc/dy)_{10\,\mathrm{K}}=-0.0095(25)$[Å/at. % Ni], which, as expected, is slightly larger but comparable to the $\hat{c}$-axis contraction rate $(dc/dy)_{300\,\mathrm{K}}=-0.0080(5)$[Å/at. % Ni] found from our powder-diffraction measurements at $T=300$ K (Fig. 1).

Fits to Sr *K*-edge data are shown in Fig. 8. While the measured La-O(2) apical distance determined from La XAFS, $r=2.36(1)$ Å, agrees with the crystallographic value $r=2.354$ Å of the undoped structure (i.e., $y=0$),[16] the local Sr-O(2) apical distance is determined from the Sr *K*-edge analysis to be $r=2.45(2)$ Å. In addition, Sr distances along the $\hat{c}$ axis show a different response to Ni doping than the response found for La distances in La XAFS. Figures 9 and 10 show the Ni-doping dependence of (La/Sr)-$(\mathrm{La/Sr})_c$ and (La/Sr)-$(\mathrm{Cu/Ni})_c$ distances and their mean-squared disorder, as obtained from La and Sr XAFS analysis. It is clear that the Sr distances along the $\hat{c}$ axis are less affected by the Ni substitution.

## IV. DISCUSSION

The local contraction of $NiO_6$ octahedra derived from the Ni XAFS and XANES measurements is most likely driven by the non-Jahn-Teller (NJT) nature of a $Ni^{2+}$ ion in its $3d^8$, high-spin, electronic configuration. This is schematically illustrated in Fig. 11, where the octahedral distortions measured by crystallography around Ni in undoped $La_2NiO_4$ and around Cu in undoped $La_2CuO_4$ are shown together with the electronic population/splitting of the $3d_{x^2-y^2}$ and $3d_{3z^2-r^2}$ energy levels in the $e_g$ manifold. Since both cuprates and nickelates have a tetragonal crystal structure, this crystal

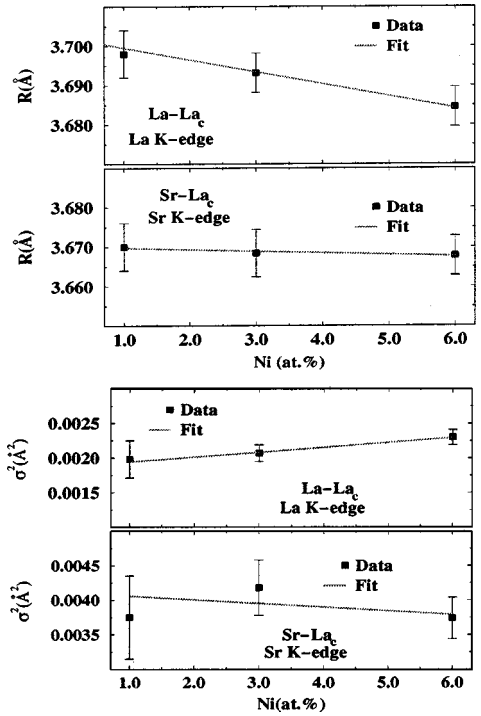


FIG. 9. Ni-doping dependence of the (La/Sr)-$La_c$ distances (top two panels) and mean-squared disorder (bottom two panels) determined from La and Sr *K*-edge XAFS analysis. The La distances respond more strongly to Ni doping than do the Sr distances.

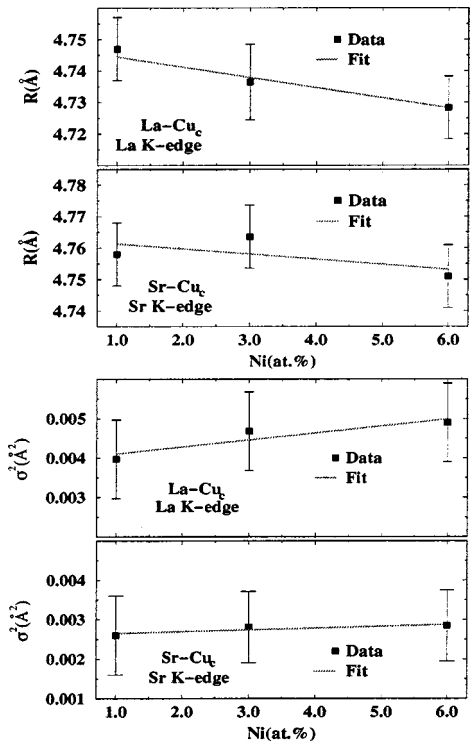


FIG. 10. Ni-doping dependence of the (La/Sr)-Cu$_c$ distances (top two panels) and mean-squared disorder (bottom two panels) determined from La and Sr *K*-edge XAFS analysis. The La distances respond more strongly to Ni doping than do the Sr distances.

field lifts the degeneracy of the $e_g$ manifold. The pseudo-Jahn-Teller (PJT) effect in $La_2CuO_4$ ($Cu^{2+}$, $3d^9$ configuration) arises due to the difference in population between $3d_{x^2-y^2}$ and $3d_{3z^2-r^2}$ energy levels; i.e., it is convenient to elongate the octahedron along the $\hat{c}$ axis (lower the energy of the doubly populated $3d_{3z^2-r^2}$ states) while compressing it in the plane (raising the energy of the singly populated $3d_{x^2-y^2}$ state by the same amount). The energy advantage in having a spontaneous elongation of the octahedra disappears in a $Ni^{2+}$ ($3d^8$) ion in its high-spin state since the occupation of $3d_{x^2-y^2}$ and $3d_{3z^2-r^2}$ $e_g$ levels is the same.

It is interesting to compare the $NiO_6$ octahedral distortion in $La_{1.85}Sr_{0.15}Cu_{1-y}Ni_yO_4$ with that in pure $La_2NiO_4$. In the latter, a fully relaxed NJT $Ni^{2+}$ ion results in a Ni-O(1) planar distance $\approx$0.04-Å longer than the Cu-O(1) distance in JT-distorted $La_2CuO_4$ (despite $Ni^{2+}$ being a smaller ion than $Cu^{2+}$). Similarly, the Ni-O(2) apical distance is $\approx$0.18-Å shorter than the Cu-O(2) one (Fig. 11). Our measurements indicate that, although the $\hat{c}$-axis contraction of Ni-O(2) in $La_{1.85}Sr_{0.15}Cu_{1-y}Ni_yO_4$ is consistent with an almost fully relaxed NJT state ($\approx$0.16 Å), the in-plane Ni-O(1) distance does not elongate by more than 0.01 Å.

The most likely explanation for this is that $NiO_6$ octahedra are embedded in the very rigid, highly covalent $CuO_2$ planes, which prevents the in-plane Ni-O(1) distance from significantly expanding and deforming the surrounding $CuO_2$ network. The much larger temperature dependence in mean-squared disorder of Ni-O(2) distance compared to Ni-O(1) is supportive of this notion. The softer Ni-O(2) bond can therefore contract without resulting in a significant elastic energy cost. The above arguments imply that a fully relaxed NJT state is not materialized for Ni in $La_{1.85}Sr_{0.15}Cu_{1-y}Ni_yO_4$.

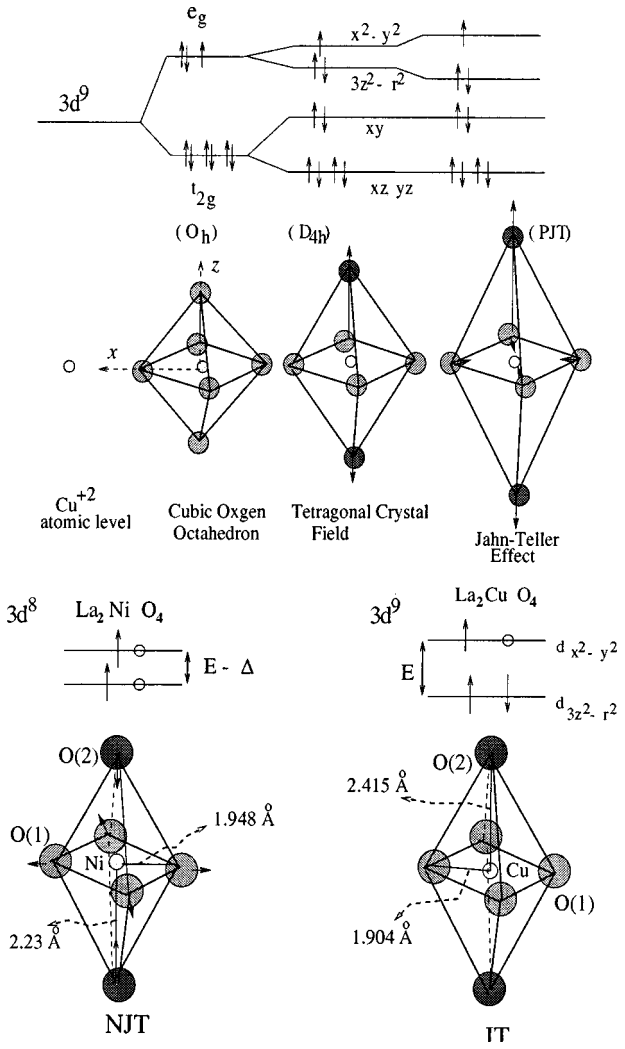


FIG. 11. Top: schematic illustration of the electronic origin of the JT effect for a $Cu^{2+}$ ion in an octahedral environment. The $e_g$ and $t_{2g}$ manifolds are split by the tetragonal crystal field and the PJT effect enhances the tetragonal distortion. Bottom: octahderal distortions in pure $La_2NiO_4$ and $La_2CuO_4$, as determined by neutron diffraction.[16,21] A closer-to-regular octahedron in the Ni case results in a smaller energy splitting of the $e_g$ manifold (represented as $\Delta$). The $NiO_6$ octahedral distortion in $La_{1.85}Sr_{0.15}Cu_{1-y}Ni_yO_4$ is very similar to that in pure $La_2NiO_4$, except that the rigid $CuO_2$ plane prevents a significant elongation of the Ni-O(1), in-plane distance to materialize.

We note that an expansion of the Ni-O(1) planar distance could in principle be accommodated by an increased buckling of the surrounding $CuO_2$ network. However, our fit results for the Ni-O(1) first shell distance and the Ni-O(1)-Cu planar buckling-angle limit such possible expansion to be $\lesssim$0.01 Å, relative to the Cu-O(1) distance.

The larger response of La-La$_c$ and La-(Cu/Ni)$_c$ distances than Sr-La$_c$ and Sr-(Cu/Ni)$_c$ to Ni doping can be understood in more than one way. One possibility is that Sr enters the lattice away from Ni sites and therefore is less sensitive to

the enhanced local lattice deformation around such sites. As mentioned earlier, the fit results of the Ni-(Sr/La) XAFS signal are consistent with such a scenario, due to the large uncertainty in the relative weight of La/Sr neighbors to Ni. Why would Sr avoid Ni? In a previous XAFS study of $La_{2-x}Sr_xCuO_4$ for a series of $x$ values below and above the insulator-metal (I-M) transition ($x \approx 0.06$ at $T=10$ K), we detected a response of the Sr-O(2) apical distance to the delocalization of doped hole carriers, while no such response was found for the La-O(2) apical distance.[23] This testifies to the fact that doped holes, introduced by the Sr dopants, are impurity states peaked in the vicinity of the Sr in the insulating phase while becoming more extended in the metallic phase. It is reasonable to argue that, if the I-M transition is caused by increased overlap of impurity states, the overlapped charge density will retain some peaking in the vicinity of the Sr even in the metallic state. A similar conclusion was reached by Hammel *et al.* in their nuclear-quadrupole-resonance study of $La_{2-x}Sr_xCuO_4$.[24] It follows that if Sr likes to attract the doped holes in its neighborhood through the $Sr^{2+}$ impurity potential, and, *if* Ni prefers to avoid them, a correlation in Ni-Sr positions may arise.

An alternative (and more likely) explanation for the different responses of Sr and La sites to Ni doping is the much weaker bonding between the O(2) apical and a $Sr^{2+}$ ion compared to a $La^{3+}$ ion. The measured Sr-O(2) apical distance (longer by $\approx 0.1$ Å) is a result of a weaker Coulomb potential felt by the negatively charged O(2) apical oxygen near a Sr ion, resulting in an equilibrium position further away from the Sr and closer to the $CuO_2$ planes. Such distortion was already reported in previous studies of $La_{2-x}Sr_xCuO_4$.[23,25] When $NiO_6$ octahedra contract and the O(2) ion is displaced towards Ni, the $La^{3+}$ ions follow the O(2) displacement, due to a significant degree of covalency in the La-O(2) bonding (the La-O(2) apical distance, 2.35 Å, is shorter than expected for a purely ionic bond). That La follows the O(2) apical is clearly seen by the measured contraction in Ni-$La_c$ distance (Table I) and in the Ni-induced contraction of the La-$(Cu/Ni)_c$ distance (Fig. 10). However, since Sr ions are more weakly bound to O(2) apicals, they should not follow as closely the O(2) apicals in their journey towards the Ni ions in the contracted $NiO_6$ octahedra, resulting in a smaller change in the Sr-$(Cu/Ni)_c$ distance relative to La-$(Cu/Ni)_c$ distance. A similar effect can also explain the behavior of (La/Sr)-$La_c$ distances. This explanation does not require a deviation from randomness in the solid solution, though it does not exclude it.

The importance of a knowledge of the local distortion induced by impurities in their neighborhood can be illustrated by discussing how it can affect the interpretation of the recent STM results on Zn and Ni impurities in a high-$T_c$ superconductor.[3,10] The theory that is used to calculate the effect of impurities is simplified by neglecting any distortions and assuming their perturbation is localized at the site of the impurity so only the $l=0$ partial-wave shift $\delta_0$ is involved. With this simplification the STM results determine separately the $\delta_0$ induced by magnetic and electrostatic effects. Only Ni has a magnetic contribution and it is found to be much weaker than the electrostatic one.[3] It is also determined that Ni is in an $S=1$ spin state consistent with our interpretation of our XAFS results. Zn has an electrostatic contribution of $|\delta_0| \approx \pi/2$ that saturates the Friedel sum rule for complete shielding of a $\Delta Z=1$ charge while the electrostatic contribution of Ni is almost as large at $|\delta_0| \approx 0.4\pi$. Here $\Delta Z$ is the difference of the $Z$ of the impurity relative to Cu, which has a magnitude of one for both Ni and Zn.

The general situation for scattering from an impurity with a distorted neighborhood requires additional phase shifts $\delta_l$ with $l=1,2,3$, etc., because the effective scattering potential is not localized in a region small compared to the carrier wavelength. When only $\delta_0$ is present the scattering-induced lifetime broadening of the carrier states is the same as the induced transport lifetime measured by resistivity since $\delta_0$ scattering is independent of angle. However, with several $\delta_l$ involved in describing the scattering these two lifetimes are not expected to be equal any longer since the transport lifetime has an additional change in carrier partial-wave velocity weighted in to the respective phase shifts to determine its value. For example, if the scattering is peaked in the forward direction the transport lifetime is longer than the phase-shift lifetime broadening. This peaked forward scattering occurs when the region of the perturbation has dimensions much greater than the carrier wavelength.

If the interpretation of the STM papers[3,10] is correct then the rate of increase in resistivity induced by Zn impurities should be somewhat greater than that of Ni. However, the experimental result is that Ni induces a significantly greater rate of increase than Zn in the La cuprates.[1] Ni also causes a metal-insulator transition at a smaller concentration than does Zn, consistent with its greater rate of inducement of resistivity. However, on the other hand, Zn is more effective than Ni in lowering $T_c$ in the La cuprates.[1] The larger $\delta_0$ of Zn versus Ni derived from the STM measurements[3,10] can explain the different rates of suppression based on an Abrikosov-Gorkov model.[26] This might indicate that these $\delta_0$ phase shifts are a good measure of the *effective* strength of the scattering despite the fact that more than one phase shift is required to understand the milder effect of Zn on transport. The total scattering phase shift dominates the $T_c$ suppression while the effect on transport includes the weighting of partial-wave velocities discussed above. For example, if the perturbation induced by Zn is distributed over a larger region than that of Ni, it will result in stronger peaking of its scattering and will result in a longer transport lifetime relative to that of Ni. XAFS measurements on Zn impurities could check this speculation.

We now turn to the implications of our findings for the mechanism(s) of $T_c$ suppression and hole localization. It is clear that the local distortion contributes to the impurity scattering potential. Although our measurements do not provide direct information on the mechanism of pair breaking by the impurity, the local atomic environment around Ni affects the degree of hybridization between $3d$ and $2p$ orbitals in $NiO_6$ octahedra relative to that in neighboring $CuO_6$ octahedra. For example, the larger $p$-$d$ charge-transfer gap in $La_2NiO_4$ compared to $La_2CuO_4$ as determined both experimentally[27–29] and theoretically[30,31] is a manifestation of the different hybridizations of $3d$-$2p$ bands in nickelates and cuprates. De-

spite Ni-O(1) and Cu-O(1) planar distances being nearly the same, the degree of hybridization between (Ni,Cu)-O(1) $3d$-$2p$ planar orbitals is not and therefore planar transfer integrals (hole hopping) at Ni sites will be modified. This has to be included in microscopic treatments. In addition, the proximity of the apical O(2) oxygen to Ni in the compressed $NiO_6$ octahedra could also contribute to pair breaking by modifying hole hopping in the out-of-plane apical direction. Such hopping is included in extended Hubbard Hamiltonians that incorporate out-of-plane orbitals,[32] but an accurate treatment should account for the local lattice distortion; i.e., the Ni-O(2) contraction.

Additional microscopic understanding into the nature of the scattering potential comes from local-density approximations (LDA)+U calculations of Anisimov *et al.* in hole-doped $La_{2-x}Sr_xNiO_4$.[33] At $x=1$, the case of $LaSrNiO_4$, a full hole charge is nominally doped per Ni site and a formal $Ni^{3+}$ valence is assumed. The calculations find that the doped holes enter *predominantly* the O $2p$ band with Ni preserving the $S=1$ high-spin configuration of undoped $La_2NiO_4$. This could explain why a ''formal'' $Ni^{3+}$ ion in $LaSrNiO_4$ has a nearly regular octahedral environment.[34] In contrast a singly populated $e_g$ shell would have resulted in a significant Jahn-Teller distortion, which is not observed. The predominant O $2p$ character for the doped holes has been confirmed by XANES measurements at the Ni $K$ edge of $LaSrNiO_4$ (Ref. 20) and $NdSrNiO_4$,[35] although some disagreement remains as to the exact ratio of Ni $3d$ to O $2p$ character for the doped hole with values in the 7% to 35% range. Predominant O $2p$ character is also concluded from O $K$-edge XANES measurements of $LaSrNiO_4$.[29]

The spin of the doped hole, distributed over neighboring oxygen sites, is expected to be strongly antiferromagnetically coupled to the localized Ni spin, increasing its effective mass.[33,30] This effective mass could be enhanced further if a lattice (polaronic) distortion is induced by the doped hole, affecting Ni-O transfer integrals. This in turn could also lead to a reduction of the spin on the Ni through the spin-bag effect.[30] Although the LDA+$U$ calculations in Ref. 30 are performed in a periodic supercell as opposed to the random distribution of Ni sites in our crystal, the issues above are relevant since they are likely active ingredients in the mechanism by which Ni induces hole localization and a metal-insulator transition at $y\approx 0.05$ in $La_{1.85}Sr_{0.15}Cu_{1-y}Ni_yO_4$. Since the calculations and experiments indicate a majority O $2p$ orbital character for the doped holes surrounding a high-spin ($S=1$) $Ni^{+2}$ ion, we expect that the strong scattering at Ni sites produces localized hole states in its vicinity but not on its site.

This is consistent with the spatial dependence of quasiparticle resonance states that are generated within the superconducting gap in the vicinity of a Ni impurity, as calculated in Refs. 8 and 9 and measured in STM experiments by Hudson *et al.*[3] It is observed that the resonant impurity bound state at the exact site of the impurity has predominantly electron character (i.e., this resonant state produces tunneling current at a positive tip bias in a STM experiment) while the resonance state at the Cu nearest neighbors to the impurity site has predominantly hole character (they produce tunneling current at a negative tip bias). It follows that the impurity potential is more attractive for electrons than for holes as the latter are bound in an impurity resonance state whose wave function has insignificant weight at the exact site of the impurity.[3,8,9] It should be noted that the STM measurement cannot determine whether the hole resonant impurity state peaks at the oxygen or copper atoms around the Ni impurities.

Since free carriers in the normal state of $La_{1.85}Sr_{0.15}CuO_4$ are of hole character, the above arguments suggest that if Ni generates impurity states for these holes their wave functions would have large amplitude in its vicinity (i.e. neighboring oxygens) but not on its site. An impurity band formed out of such states would be half filled and lead to insulating behavior, assuming strong repulsion between holes. The possibility of such a Mott-Hubbard transition in an impurity band has been proposed, but a revision of the Mott criterion for the case of strongly anisotropic impurity states, as in a $d$-wave superconductor, is still needed.[36] In contrast to this model, the localization of carriers by Ni and Zn impurities is commonly interpreted in the context of Anderson's theory of disorder-induced localization, although the presence of a Coulomb gap was previously postulated based on resistivity measurements in the insulating regime.[1]

The lattice distortion (and related changes in transfer integrals) together with magnetic confinement of doped holes via exchange coupling to the high-spin Ni sites results in strong scattering leading to increased residual resistivities and hole localization at $y\approx 0.05$. This in turn results in an inhomogeneous charge distribution in the normal state. It is possible that these local interactions compete with pairing interactions at the microscopic level inhibiting pair formation around Ni dopants. However, the STM experiments indicate, for the very dilute case, that superconductivity remains unaltered at the location of Ni impurities, judging by the robust SC coherence peaks and gap observed at these sites.[3] This is in contrast to the case of Zn (Ref. 10) and the ''swiss cheese'' model of Nachumi *et al.*,[37] where the effect of dopants is to remove superconducting pairs from the superfluid in a $\pi\zeta_{ab}^2$ region around the dopants.

We note that both Ni and Zn doping in La cuprates contract the crystallographic $c/a$ ratios at nearly identical rates.[38] This is expected from the non-Jahn-Teller nature of a $Zn^{2+}$ ion, which should result in a very similar octahedral contraction as reported here for Ni. XAFS measurements at the Zn sites of doped cuprates should confirm or invalidate this assumption. Until such information is available one cannot rule out the possibility of different lattice distortions around Zn and Ni contributing to the faster rate of $T_c$ suppression with Zn doping.

The spatial extent of a superconducting wave function cannot be confined to a region smaller than its coherence length, as the resulting quasiparticle localization energy would be larger than the superconducting energy gap. It is interesting to note that $T_c$ is completely suppressed at 3–4-at. % Ni, where the average distance between Ni dopants in the two-dimensional $CuO_2$ planes is $3.78/\sqrt{y}\approx 19-22$ Å. This is about the size of the in-plane superconducting coherence length, $\zeta_{ab}=22.7$ Å for $La_{1.85}Sr_{0.15}CuO_4$.[37] It is then

possible that superconductivity is destroyed when the superconducting state is constrained to occupy regions of the $CuO_2$ plane in between Ni centers, which, for $y \gtrsim 0.03$, are smaller than $\zeta_{ab}$.

## V. CONCLUSIONS

We have shown here that a strong lattice distortion exists around the Ni atoms in $La_{1.85}Sr_{0.15}Cu_{1-y}Ni_yO_4$. The local Ni-O distances in the $NiO_6$ octahedra are very similar to those in $La_2NiO_4$. Based on this similarity and on theoretical calculations of the electronic structure of Ni in related compounds we conclude that the Ni impurities are in a high-spin $S=1$ non-Jahn-Teller state. The local distortion manifests a large $\hat{c}$-axis contraction of the $NiO_6$ octahedra, which propagates to higher shells of neighboring atoms along the $\hat{c}$ axis. This has implications for the interpretation of spectroscopies that are sensitive to spatially inhomogeneous local $\hat{c}$-axis distortions. For example, the local tunneling cross sections,[10] which depend on the local interlayer spacing, will vary from a Ni-dopant site to a neighboring Cu site due to the local $\hat{c}$-axis fluctuations.

The Sr and La environments respond differently to Ni doping. Although this could be explained as due to Ni entering the lattice away from Sr sites, a more likely explanation involves a weaker Sr-O(2) apical bond compared to a stronger La-O(2) apical bond. The latter results in La ions ''following'' more faithfully the O(2) apical distortion toward Ni ions, while the Sr ions are not as affected due to their weaker link to the O(2) apicals.

The scattering potential at the Ni sites has a contribution from its induced local distortion which is expected to introduce a perturbation in its electrostatic potential that cannot be described by a single partial-wave phase shift. As discussed this feature could explain the different rates of change in $T_c$ and resistivity with Ni and Zn doping in La cuprates and the different concentrations at which the M-I transition occurs. Superconductivity is fully suppressed when the average distance between Ni dopants is on the order of the in-plane superconducting coherence length. This is expected if the superconducting wave function is confined to the regions in between Ni dopants, as its spatial extent cannot be smaller than the superconducting coherence length.

Our results show that the improved understanding of the local atomic environment around Ni dopants provides new insights into the mechanisms of $T_c$ suppression and hole localization by Ni dopants in $La_{1.85}Sr_{0.15}Cu_{1-y}Ni_yO_4$.

## ACKNOWLEDGMENTS

It is a pleasure to acknowledge Frank Perez and Mas Suenaga for their help with the magnetic alignment of powders, Arnie Moodenbaugh for the $T_c$ measurements, and Zahirul Islam and Eric Hudson for a critical reading of this manuscript. Research was done under auspices of DOE Grant No. DE-FG03-98ER45681. D.H. was also partially supported by DOE Contract No. W-31-109-Eng-38.

[1] M. Z. Cieplak, S. Guha, H. Kojima, P. Lindenfeld, G. Xiao, J. Q. Xiao, and C. L. Chien, Phys. Rev. B **46**, 5536 (1992).
[2] M. I. Salkola, A. V. Balatsky, and J. R. Schrieffer, Phys. Rev. B **55**, 12 648 (1997).
[3] E. Hudson, K. M. Lang, V. Madhaven, S. H. Pan, H. Eisaki, S. Uchida, and J. C. Davis, Nature (London) **411**, 920 (2001).
[4] J. M. Byers, M. E. Flatte, and D. J. Scalapino, Phys. Rev. Lett. **71**, 3363 (1993).
[5] M. I. Salkola, A. V. Balatsky, and D. J. Scalapino, Phys. Rev. Lett. **77**, 1841 (1996).
[6] C. Huscroft and R. T. Scalettar, Phys. Rev. Lett. **81**, 2775 (1998).
[7] C. Pépin and P. A. Lee, Phys. Rev. Lett. **81**, 2779 (1998).
[8] I. Martin and A. V. Balatsky, cond-mat/0003142 (unpublished).
[9] S. Haas and K. Maki, Phys. Rev. Lett. **85**, 2172 (2000).
[10] S. H. Pan, E. W. Hudson, K. M. Lang, H. Eisaki, S. Uchida, and J. C. Davis, Nature (London) **403**, 746 (2000).
[11] A. V. Balatsky, Nature (London) **403**, 717 (2000).
[12] D. Haskel, E. A. Stern, F. Dogan, and A. R. Moodenbaugh, Phys. Rev. B **61**, 7055 (2000).
[13] E. A. Stern, M. Newville, B. Ravel, Y. Yacoby, and D. Haskel, Physica B **208 & 209**, 117 (1995).
[14] S. I. Zabinsky, J. J. Rehr, A. Ankudinov, R. C. Albers, and M. J. Eller, Phys. Rev. B **52**, 2995 (1995).
[15] M. Newville, B. Ravel, D. Haskel, J. J. Rehr, E. A. Stern, and Y. Yacoby, Physica B **208 & 209**, 154 (1995).
[16] P. G. Radaelli, D. G. Hinks, A. W. Mitchell, B. A. Hunter, J. L. Wagner, B. Dabrowski, K. G. Vandervoort, H. K. Viswanathan, and J. D. Jorgensen, Phys. Rev. B **49**, 4163 (1994).
[17] We note that determining the Sr-Ni correlation from Sr *K*-edge XAFS is not possible, due to the nearly identical backscattering amplitudes of Ni and Cu atoms.
[18] H. Oyanagi, Y. Yokoyama, H. Yamaguchi, Y. Kuwuahara, Y. Katayama, and Y. Nishihara, Phys. Rev. B **42**, 10 136 (1990).
[19] N. Kosugi, Y. Tokura, H. Tajima, and S. Uchida, Phys. Rev. B **41**, 131 (1990).
[20] A. Sahiner, M. Croft, S. Guha, I. Perez, Z. Zhang, M. Greenblatt, P. A. Metcalf, H. Jahns, and G. Liang, Phys. Rev. B **51**, 5879 (1995).
[21] J. Rodriguez-Carvajal, M. T. Fernandez-Diaz, and J. L. Martinez, J. Phys.: Condens. Matter **3**, 3215 (1991).
[22] D. Haskel, Ph. D. thesis, University of Washington, 1998.
[23] D. Haskel, E. A. Stern, and F. Dogan, in *Phase Transitions and Self Organization in Electronic and Molecular Networks*, Fundamental Materials Research Series, edited by M. F. Thorpe and J. C. Phillips (Kluwer Academic/Plenum, New York, in press).
[24] P. C. Hammel, B. W. Statt, R. L. Martin, F. C. Chou, D. C. Johnston, and S. W. Cheong, Phys. Rev. B **57**, R712 (1998).
[25] D. Haskel, E. A. Stern, F. Dogan, and A. R. Moodenbaugh, J. Synchrotron Radiat. **8**, 186 (2001).
[26] A. A. Abrikosov and L. P. Gorkov, Zh. Éksp. Teor. Fiz. **39**, 1781 (1960) [Sov. Phys. JETP **12**, 1243 (1961)].
[27] S. L. Cooper, G. A. Thomas, A. J. Millis, P. E. Sulewski, J. Oren-

stein, D. H. Rapkine, S-W. Cheong, and P. L. Trevor, Phys. Rev. B **42**, 10 785 (1990).
[28] J. Orenstein, G. A. Thomas, D. H. Rapkine, C. G. Bethea, B. F. Levine, B. Battlog, R. J. Cava, D. W. Johnson, and E. A. Rietman, Phys. Rev. B **36**, 8892 (1987).
[29] P. Kuiper, J. van Elp, G. A. Sawatzky, A. Fujimori, S. Hosoya, and D. M. de Leeuw, Phys. Rev. B **44**, 4570 (1991).
[30] V. I. Anisimov, M. A. Korotin, J. Zaanen, and O. K. Andersen, Phys. Rev. Lett. **68**, 345 (1992).
[31] J. B. Grant and A. K. McMahan, Phys. Rev. Lett. **66**, 488 (1991).
[32] L. F. Feiner, M. Grilli, and C. Di Castro, Phys. Rev. B **45**, 10 647 (1992).
[33] V. I. Anisimov, D. Bukhvalov, and T. M. Rice, Phys. Rev. B **59**, 7901 (1999).
[34] P. J. Heaney, A. Mehta, G. Sarosi, V. E. Lamberti, and A. Navrotsky, Phys. Rev. B **57**, 10 370 (1998).
[35] Z. Tan, S. M. Heald, S-W. Cheong, A. S. Cooper, and A. R. Moodenbaugh, Phys. Rev. B **47**, 12 365 (1993).
[36] A. V. Balatsky, M. I. Salkola, and A. Rosengren, Phys. Rev. B **51**, 15 547 (1995).
[37] M. E. Nachumi, A. Keren, K. Kojima, M. Larkin, G. M. Luke, J. Merrin, O. Tchernyshöv, Y. J. Uemura, N. Ichikawa, M. Goto, and S. Uchida, Phys. Rev. Lett. **77**, 5421 (1996).
[38] X. Gaojie, M. Zhiqiang, T. Mingliang, W. Yu, and Z. Yuheng, J. Supercond. **10**, 13 (1997).